fluids

MDPI

Article

Simulation and Analysis of Heat Loss in Steam Injection Pipelines Considering Sunlight Radiation and Installation Methods

Paerhati Abudukelimu [1], Junde Liu [2], Genying Gao [1], Jianping Zhou [1], Yan Qiao [3,*], Zhongshan Ma [1] and Xinwei Wang [3]

[1] Research Institute of Oil Production Technology, Petro China Xinjiang Oilfield Company, Karamay 834000, China; pahat@petrochina.com.cn (P.A.); gaogy2@petrochina.com.cn (G.G.); zgskfs_zjp@petrochina.com.cn (J.Z.); mazhongshan@petrochina.com.cn (Z.M.)
[2] Infrastructure Engineering Department, Petro China Xinjiang Oilfield Company, Karamay 834000, China; ptrljd@petrochina.com.cn
[3] College of New Energy, China University of Petroleum (East China), Qingdao 266580, China; wangxw@upc.edu.cn
* Correspondence: qiaoyan_1110@163.com; Tel.: +86-15141219897

Abstract

Heat loss in steam injection pipelines is one of the primary causes of low thermal efficiency in heavy oil steam injection. To investigate the heat loss and heat transfer variation patterns in steam injection pipelines, a three-dimensional numerical model was established using Fluent software. The effects of overhead pipeline insulation parameters and environmental factors on heat loss and radial temperature distribution were analyzed. This study systematically quantifies the effects of sunlight radiation for the first time and proposes a heat loss correction equation for sunlight conditions. Additionally, overhead and buried pipelines were compared within the same modeling framework. The results show that selecting insulation materials with low thermal conductivity and increasing the insulation thickness can effectively reduce steam pipeline heat loss. For overhead pipelines, as sunlight radiation intensity increased from 0 W/m^2 to 800 W/m^2, actual heat loss decreased from 68.43 W/m^2 to 58.03 W/m^2. A sunlight-dependent effective heat transfer coefficient, h_{Sunlight} (E, T), was fitted to extend surface temperature heat loss calculations under sunlightt conditions, in which determination (R^2) is 0.9951 and the average error is 5.57%. Under the same operating conditions, the heat loss of the buried pipelines was 62.59 W/m^2, which was 8.5% lower than that of the overhead pipelines. The findings provide a theoretical basis for the insulation design, thermal efficiency assessment, and operational optimization under sunlight radiation conditions of steam injection pipelines.

Keywords: heavy oil extraction; steam injection pipelines; heat transfer; heat loss; sunlight intensity

Check for updates

Academic Editor: Wenning Zhou

Received: 13 June 2026
Revised: 8 July 2026
Accepted: 9 July 2026
Published: 11 July 2026

Copyright: © 2026 by the authors. Licensee MDPI, Basel, Switzerland. This article is an open access article distributed under the terms and conditions of the Creative Commons Attribution (CC BY) license.

1. Introduction

Heavy oil, as a critical unconventional hydrocarbon resource, plays a vital role in global energy supply [1–3]. Overcoming the technological bottleneck of heavy oil extraction is a huge challenge for the global oil industry; it is also a strategic issue concerning future energy supply security and technological innovation [4–6]. Steam injection thermal recovery is widely adopted to reduce oil viscosity and enhance mobility [7]. However, heat loss during steam injection directly impacts thermal efficiency and operational costs, especially

in overhead and buried pipelines [8–10]. The complexity of heat loss mechanisms arises from pipeline structures, insulation material properties, and environmental factors [11,12]. Understanding the underlying heat transfer mechanisms and characteristics is essential for accurately predicting and reducing heat loss [13–15]. Reducing heat loss and optimizing thermal utilization remain key challenges in heavy oil thermal recovery.

Previous studies have examined the impact of thermal insulation materials on heat transfer characteristics. Ananda et al. [16] calculated the heat loss and cost of different insulation materials with different thicknesses for steam pipelines using mineral wool, cement, and lead as insulation materials and carried out a detailed heat transfer analysis for steam pipelines with different pipeline diameters. Lin et al. [17] conducted a field test study on the heat loss characteristics of overhead pipelines of 12 different types of steam heating networks with an operating time of 1~11 years and analyzed the mechanism of thermal insulation degradation in terms of both material degradation and structural deformation. Wang [18] proposed methods to control the temperature drop and heat loss along heat transfer pipelines, such as doubling the thickness of the insulation layer or reducing the thermal conductivity by half, which can reduce the heat loss of the pipelines by 50%, and analyzed in detail the reasons for these results. Příhoda et al. [19] conducted mathematical and physical analyses of heat losses in insulated versus uninsulated pipes within outdoor heat distribution systems. Alrasheed [20] used a multi-objective genetic algorithm to optimize the thickness of multi-layer insulation around pipes carrying fluids, with the aim of minimizing heat loss and associated costs.

Some scholars have proposed novel methods for calculating heat loss in pipelines. Kruczek [21] presented a new methodology applicable to the determination of annual heat loss in large and complex thermal or steam pipelines. Danielewicz et al. [22] proposed an innovative method using numerical modeling and field measurements to identify heat losses in underground heating networks under transient conditions and quantify their surrounding temperature distributions. Bøhm [23] developed a novel approach to determine undisturbed ground temperatures by calculating transient heat losses through steady-state heat loss equations.

Existing research has only considered the impact of insulation layer parameters on pipeline heat loss, neglecting the influence of sunlight. For buried pipelines, only heat loss calculation methods have been proposed, without comparison to overhead pipelines. Furthermore, the current national standard of China (GB) overlooks the effect of sunlight radiation on outer-wall temperatures, leading to evaluation discrepancies. Notably, the difference in heat loss between overhead and buried pipelines lacks theoretical support grounded in engineering practice.

To address the aforementioned challenges, this study develops a three-dimensional heat transfer model for steam injection pipelines and utilizes Fluent software to simulate and explore heat loss processes and heat transfer mechanisms under varying operational conditions. By comparatively analyzing the effects of pipeline parameters (insulation thermal conductivity, thickness, steam temperature), environmental factors (ambient temperature, sunlight radiation), and installation methods (overhead or buried) on the heat transfer rate, the key controlling factors of heat loss are systematically identified. The innovation of this paper is threefold: (1) it systematically quantifies the positive effects of sunlight radiation for the first time; (2) it proposes a practical correction formula for sunlight conditions; and (3) it compares overhead and buried pipelines within a unified modeling framework. The dynamic impact of sunlight intensity on the outer-wall temperature and heat loss is quantitatively revealed, and a formula for calculating heat loss under sunlight conditions is established. Furthermore, by comparing the heat loss and heat transfer characteristics of overhead and buried pipelines, as well as buried pipelines

with and without insulation layers, the study elucidated the mechanisms by which soil conditions and insulation structures influence heat loss in buried steam injection pipelines. The research content schematic diagram is shown in Figure 1. The research outcomes provide theoretical support for optimizing pipelines structural design, insulation material selection, and construction strategies, offering significant engineering value for advancing the green and efficient extraction of heavy oil resources.

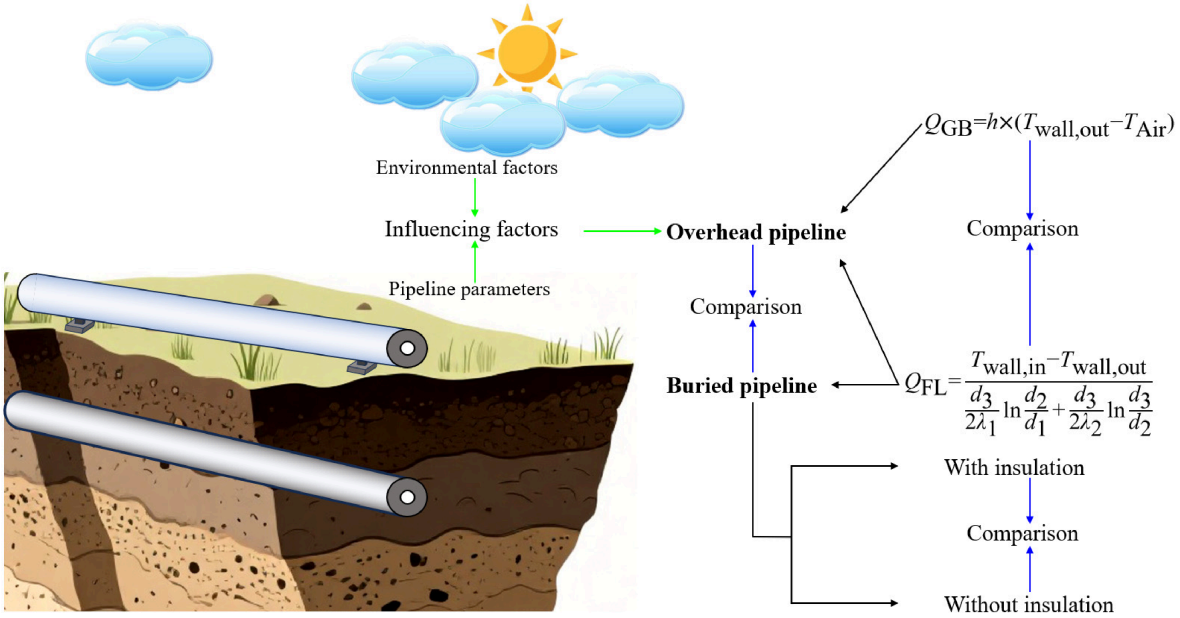


Figure 1. Research content schematic diagram.

2. Model Establishment

2.1. Physical Model

The geometric model of the steam injection pipeline is shown in Figure 2. The pipeline and insulation materials are modeled as homogeneous media with constant properties. The realizable k-ε turbulence model was selected to simulate natural convective heat transfer from the outer wall of the overhead pipe to the ambient air. The Rosseland radiation model was adopted to account for radiative heat transfer. The boundary condition of the inner wall of the pipeline was set as a constant temperature; the temperature value is equal to the steam temperature. The boundary conditions of the outer wall of the insulation layer were convective heat transfer and radiative heat transfer. The value of the heat transfer coefficient in the convective condition is referred to in Equation (8). The sunlight radiation intensity was converted according to the Stefan–Boltzmann law [24]. Basic parameters and initial conditions are listed in Table 1. The boundary conditions of the other walls were set to be system-coupled. This study is based on the finite volume method and utilizes ANSYS 2022R1 Fluent software. In the surrounding air domain, the continuity, momentum, turbulence, and energy equations were solved to describe natural convection around the pipeline. The SIMPLE algorithm was employed for pressure–velocity coupling; the convection terms in the air-domain momentum and energy equations were discretized using a second-order upwind scheme. In the solid regions, including the pipe wall and insulation layer, only the steady-state heat conduction equation was solved. The internal steam flow was not explicitly simulated and is represented by a constant-temperature boundary condition at the inner wall of the pipeline. Iterative calculations were performed, with convergence defined as the residuals at key monitoring points falling below 10^{-6}.

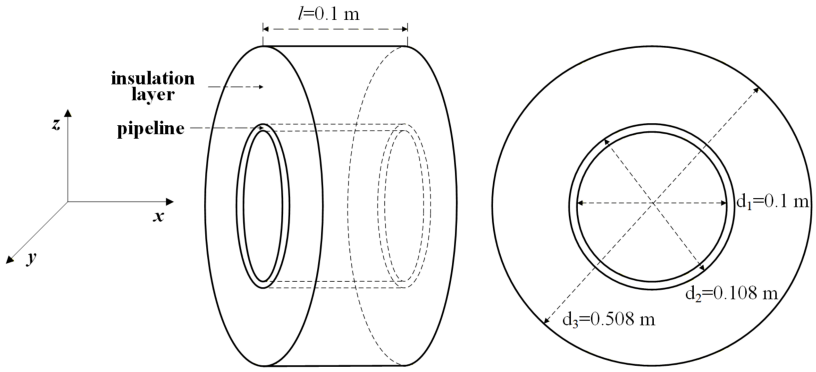


Figure 2. Geometric model of the steam injection pipeline.

Table 1. Basic parameters and initial conditions.

Parameter	Value
Pipeline inner diameter (m)	0.1
Pipeline outer diameter (m)	0.108
Insulation thickness (m)	0.2
Steam temperature (K)	573.15
Ambient temperature (K)	298.15
Pipeline thermal conductivity (W/(m·K))	45
Insulation thermal conductivity (W/(m·K))	0.1
Burial depth of buried pipelines (m)	1.8
Soil thermal conductivity (W/(m·K))	0.8

2.2. Grid Independence Verification

The computational grid of the steam injection pipeline was divided using the IEM CFD module; the grid near the boundary layer was locally densified to ensure that the dimensionless height $y^+ < 1$. Five sets of grids with the quantities of 141,603, 163,186, 186,135, 215,310, and 238,291 were divided. Numerical simulations were conducted under the same working conditions; the comparison results of the wall temperature distribution are shown in Figure 3. It was found that when the grid quantity was 186,135, further refinement of the grid would not cause any changes in the simulation results, indicating that grid 3 has both computational efficiency and simulation accuracy, and can be used for the numerical calculations in this paper. The division of grid 3 is shown in Figure 4a. The grid of the buried pipeline is based on the overhead pipeline, and the soil area is added. According to the burial depth, the soil thickness from the pipeline center to the ground surface is set to 1.8 m, and the soil thickness on the left, right, and bottom sides of the pipeline is 5 m. The boundary conditions of the soil area in contact with the pipeline are thermal conduction, the soil boundary condition above the pipeline in contact with the air is convective heat transfer, and the soil boundary conditions on the left, right, and bottom sides are insulation. The grids of the buried pipeline and the soil are shown in Figure 4b.

2.3. Model Validation

To validate the reliability of this model, the numerical results were compared with field data, where the fluid temperature inside the pipe was 561.65 K. The validation data were obtained from the overhead steam injection pipeline at the Xinjiang Oilfield. The outer surface temperature of the pipeline was measured using a handheld thermocouple with an accuracy of ±0.5 K. Three measurements were taken and the average value was used. The measurements were conducted at night under windless and dark conditions. The comparison results are shown in Figure 5. It can be observed that the simulated results

and experimental results exhibit good agreement, with an average error of 0.75%. This indicates that the numerical method employed in this study is accurate and reliable.

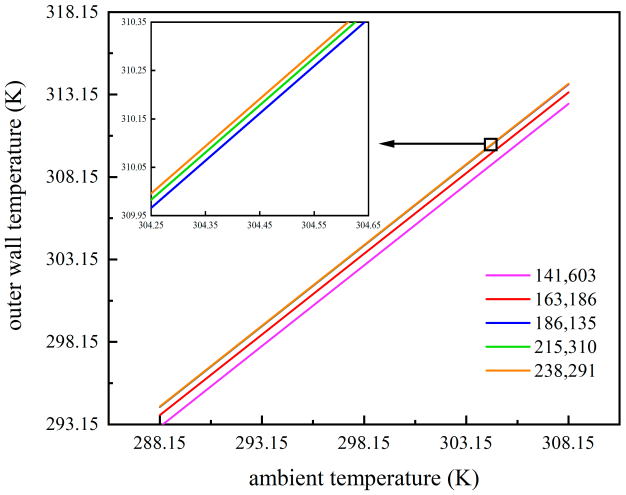
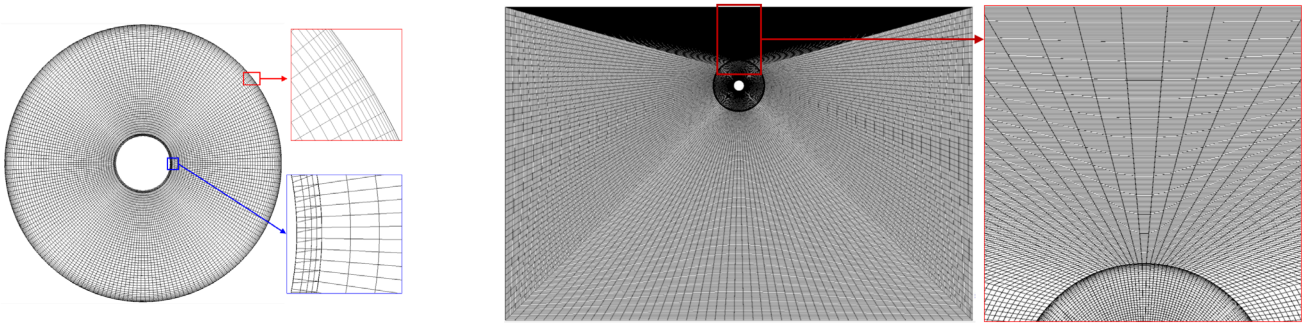


Figure 3. Mesh independence verification.



(**a**) Overhead pipeline (**b**) Buried pipeline

Figure 4. Cross-sectional view of the pipeline grid generation.

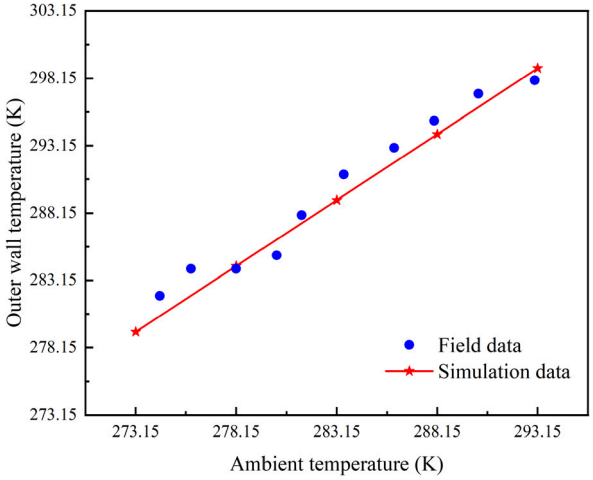


Figure 5. Simulation and field data validation.

2.4. Conditional Assumption

(1) The model operates in steady state, eliminating axial temperature gradients;

(2) Ignoring fluid flow and heat exchange within the pipeline, the inner wall temperature of the pipeline is equal to the steam temperature;

(3) Sunlight irradiation is treated as an equivalent thermal radiation flux using the Stefan–Boltzmann law, assuming a surface absorptivity of 0.85.

2.5. Control Equations

The computational domain consists of the surrounding air domain and the solid domains, including the pipe wall and the insulation layer. The surrounding air domain is used to describe natural convection around the pipeline, whereas the solid domains are used to describe heat conduction through the pipe wall and insulation layer. The internal steam flow is not explicitly solved in this study; instead, the steam side is represented by a constant-temperature boundary condition imposed on the inner wall of the pipeline.

For the surrounding air domain, the three-dimensional steady-state governing equations include the continuity, momentum, and energy equations.

The continuity equation is expressed as:

$$\frac{\partial u}{\partial x} + \frac{\partial v}{\partial y} + \frac{\partial w}{\partial z} = 0 \tag{1}$$

where u, v, and w are velocity components in the x, y, and z directions.

The momentum equation for the air domain can be written as:

$$\rho(u\cdot\nabla)u = -\nabla p + \nabla\cdot[(\mu + \mu_t)(\nabla u + \nabla u^T)] + \rho g \tag{2}$$

where ρ is the air density, kg/m^3; u is the velocity vector, m/s; p is the pressure, Pa; μ is the dynamic viscosity, Pa·s; μ_t is the turbulent viscosity, Pa·s; and g is the gravitational acceleration vector, m/s^2. The realizable k-ε turbulence model is adopted to describe the turbulent natural convection in the surrounding air.

The energy equation for the air domain is expressed as:

$$\rho c_p \left(u\frac{\partial T}{\partial x} + v\frac{\partial T}{\partial y} + w\frac{\partial T}{\partial z} \right) = \nabla\cdot[(\lambda + \lambda_t)\nabla T] + S_r \tag{3}$$

where c_p is the specific heat capacity of air, J/(kg·K); T is the temperature, K; λ is the thermal conductivity of air, W/(m·K); λ_t is the turbulent thermal conductivity, W/(m·K); and S_r is the radiation source term. The Rosseland radiation model is used to account for radiative heat transfer in the air domain.

For the solid domains, including the pipe wall and the insulation layer, only heat conduction is considered. Therefore, the steady-state energy equation is written as:

$$\nabla\cdot(\lambda_s \nabla T) = 0 \tag{4}$$

where λ_s is the thermal conductivity of the solid material, W/(m·K). For the pipe wall, $\lambda_s = \lambda_1$; and for the insulation layer, $\lambda_s = \lambda_2$.

The temperature and heat flux are coupled at the interfaces between different regions. At the pipe wall–insulation interface and the insulation–air interface, the following conditions are satisfied:

$$T_1 = T_2 \tag{5}$$

$$-\lambda_1 \frac{\partial T_1}{\partial n} = -\lambda_2 \frac{\partial T_2}{\partial n} \tag{6}$$

where n denotes the normal direction of the interface.

The SIMPLE algorithm is employed for pressure–velocity coupling in the air domain. The convection terms in the air-domain momentum and energy equations are discretized using a second-order upwind scheme. It should be noted that the convection

terms exist only in the surrounding air domain. In the pipe wall and insulation layer, the energy equation contains only the heat conduction term and, therefore, does not involve convective discretization.

2.6. Calculation Methods

The current national standard method of China for heat loss calculation (GB/T 17357-2008, in situ measurements of heat loss through thermal insulation of equipments and pipes–heat flow meter apparatus and surface temperature method) was used [25]:

$$Q_{GB} = h_{GB}(T_{wall,out} - T_{Air}) \tag{7}$$

$$h_{GB} = 11.63 + 7.0\sqrt{\omega} \tag{8}$$

where Q is the heat loss per unit area, W/m^2; h is the heat transfer coefficient, W/(m^2·K); and ω is wind speed, $\omega \leq 0.5$ m/s.

Fourier's law for cylindrical heat conduction was used [26]:

$$Q_{FL} = \frac{\varphi}{A} = \frac{T_{wall,in} - T_{wall,out}}{\frac{d_3}{2\lambda_1}\ln\frac{d_2}{d_1} + \frac{d_3}{2\lambda_2}\ln\frac{d_3}{d_2}} \tag{9}$$

$$\varphi = \frac{2\pi L(T_{wall,in} - T_{wall,out})}{\frac{1}{\lambda_1}\ln\frac{d_2}{d_1} + \frac{1}{\lambda_2}\ln\frac{d_3}{d_2}} \tag{10}$$

$$A = \pi d_3 l \tag{11}$$

where φ denotes the heat flux, W; the subscript "wall,in" indicates the pipeline inner wall temperature, the subscript "wall,out" indicates the insulation outer-wall temperature, K; d_1, d_2, and d_3 represent the pipeline inner diameter, pipeline outer diameter, and insulation outer diameter, m, respectively; λ_1 and λ_2 correspond to the thermal conductivity of the pipeline and insulation layer, W/(m·K), respectively; and A represents area, m^2.

The deviation (ε) between the GB and Fourier methods is as follows:

$$\varepsilon = |Q_{FL} - Q_{GB}| \times 100\% \tag{12}$$

3. Results and Discussion

Numerical simulations were conducted to investigate the heat transfer characteristics of overhead steam injection pipelines. Heat loss in the pipelines was calculated and compared using the GB method and Fourier's cylindrical heat conduction method. The effects of insulation thermal conductivity, insulation thickness, steam temperature, ambient temperature, and sunlight radiation on heat transfer and heat loss were systematically analyzed. Additionally, a comparative analysis was performed between overhead and buried steam pipelines. Sections 3.1–3.5 apply to overhead pipelines and the grid model is for overhead pipeline model; while Sections 3.6–3.8 apply to buried pipelines, and the grid model is for the buried pipeline model. Key findings from the detailed analysis are summarized as follows.

3.1. Insulation Thermal Conductivity

The influence of thermal conductivity of insulation layer on heat loss is shown in Figure 6. The Q_{FL} (Fourier's law heat loss) value is slightly higher than Q_{GB} (surface temperature method heat loss, GB/T 17357-2008); both Q_{FL} and Q_{GB} gradually increase with the rising thermal conductivity of the insulation layer, while ε progressively decreases. Figure 7 illustrates radial temperature distributions for different insulation thermal conductivities, where the green area represents the pipes and the blue area denotes the insulation

layers. As pipeline thickness increases, the radial temperature gradually decreases. Due to the pipeline's thin wall thickness and high thermal conductivity compared to the insulation layer's thick wall and low thermal conductivity, the temperature drop within the pipeline remains relatively small while showing significant a reduction across the insulation layer. Simultaneously, the enhanced thermal conductivity of the insulation layer strengthens heat transfer capacity, leading to gradual increases in Q_{FL}. The outer-wall temperature of the insulation layer rises with higher thermal conductivity, enlarging the temperature difference with the ambient environment and consequently increasing Q_{GB}. The growth rate of Q_{FL} is less pronounced than that of Q_{GB}, resulting in a gradual decrease in ε. When the insulation thermal conductivity λ_2 is 0.05 W/(m·K), ε reaches 0.86%, which decreases to 0.51% when λ_2 is 0.15 W/(m·K). For every 0.01 W/(m·K) increase in the thermal conductivity of insulation materials, heat loss increases by 6.7 W/m^2. Higher thermal conductivity accelerates the heat transfer rate, while lower values indicate better insulation performance. Therefore, selecting insulation materials with lower thermal conductivity can effectively reduce heat loss in steam injection pipelines.

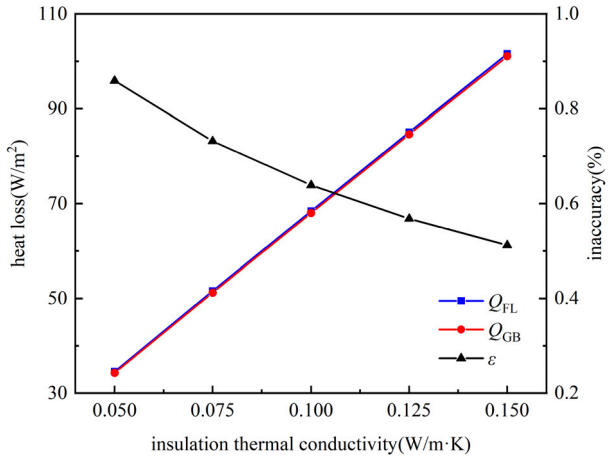


Figure 6. Effect of insulation thermal conductivity on heat loss.

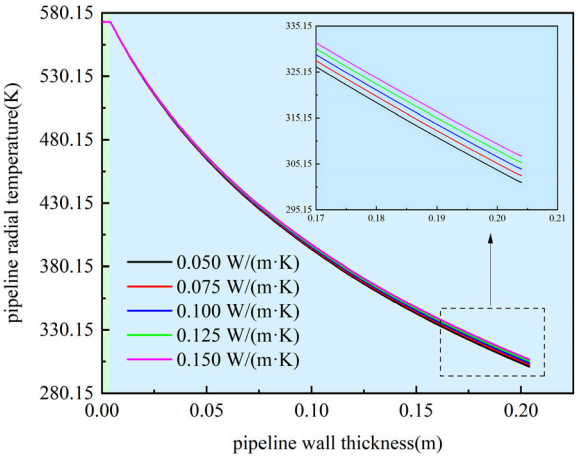


Figure 7. Radial temperature distributions for different insulation thermal conductivity.

3.2. Insulation Thickness

The influence of insulation thickness on heat loss is shown in Figure 8. The Q_{FL} value slightly exceeds Q_{GB}, with both parameters gradually decreasing as insulation thickness increases, while ε progressively rises. Figure 9 demonstrates radial temperature distributions under varying insulation thicknesses. As insulation thickness increases, the heat transfer

path length from the pipeline's inner wall to the insulation outer surface extends, resulting in a reduced heat transfer rate and consequent gradual decrease in Q_{FL}. When insulation thickness increases from 0.2 m to 0.3 m, the outer surface temperature of the insulation layer decreases from 304 K to 301.63 K, thereby reducing the temperature difference with the ambient environment and lowering the heat loss from 68.43 W/m^2 to 40.79 W/m^2. As the insulation thickness increases from 0.20 m to 0.25 m, the incremental reduction in heat loss is 3.38 W/m^2 per 0.01 m, which decreases to 2.14 W/m^2 per 0.01 m for thicknesses from 0.25 m to 0.30 m, indicating a diminishing return. The greater insulation thickness corresponds to the lower heat transfer rate. Therefore, increasing insulation thickness within economic feasibility and spatial constraints can effectively reduce heat loss in pipelines.

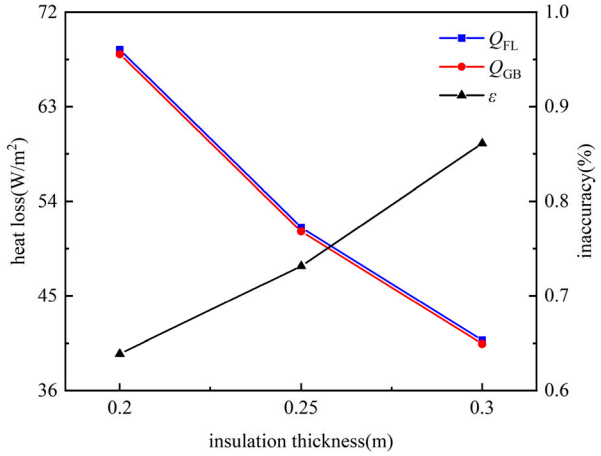


Figure 8. Effect of insulation thickness on heat loss.

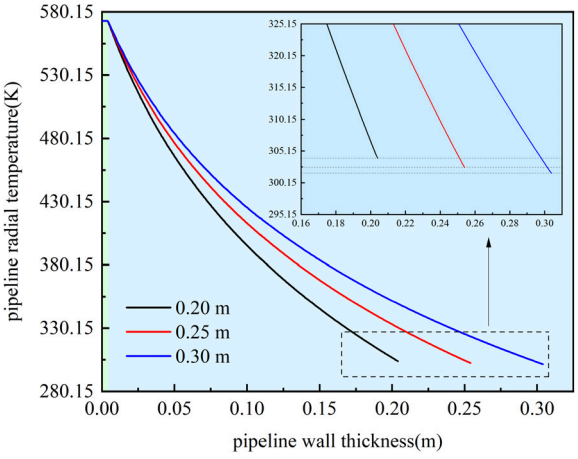


Figure 9. Radial temperature distributions for different insulation thicknesses.

3.3. Steam Temperature

The influence of steam temperature on heat loss is shown in Figure 10. The Q_{FL} value slightly exceeds Q_{GB}, with both parameters gradually increasing as steam temperature rises, while ε remains constant at 0.64%. Figure 11 demonstrates radial temperature distributions at different steam temperatures. Elevated steam temperature raises the outer-wall temperature of the insulation layer, thereby increasing both Q_{FL} and Q_{GB}. Notably, these parameters exhibit identical growth rates under temperature elevation, maintaining ε consistently at 0.64%. For every 10 K increase in steam temperature, heat loss increases by 2.49 W/m^2. In practical applications, the effect of steam temperature on pipeline material performance should be carefully considered, as excessively high temperatures may lead to material degradation and phase transition risks, posing potential safety concerns.

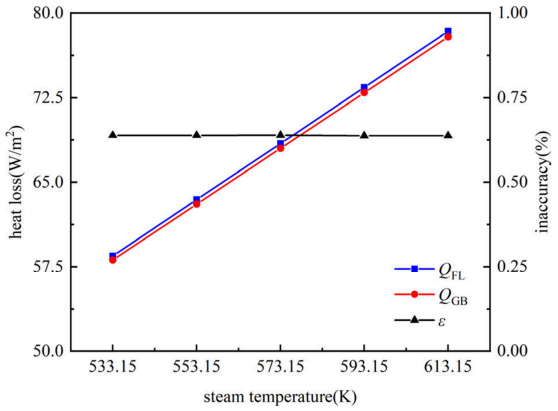


Figure 10. Effect of steam temperature on heat loss.

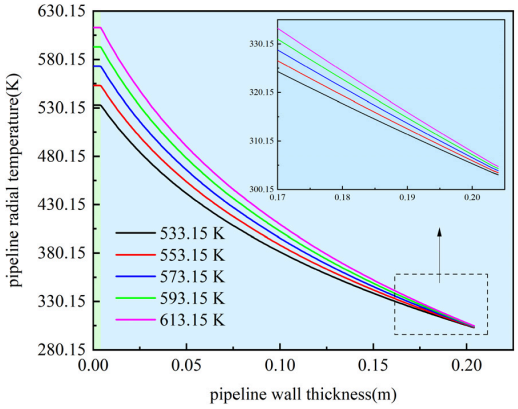


Figure 11. Radial temperature distributions at different steam temperatures.

3.4. Ambient Temperature

The influence of ambient temperature on heat loss is shown in Figure 12. The Q_{FL} value slightly exceeds Q_{GB}, with both parameters gradually decreasing as ambient temperature rises, while ε remains constant at 0.64%. Figure 13 illustrates radial temperature distributions at different ambient temperatures. The elevated ambient temperature raises the baseline temperature of the insulation layer's outer surface, which diminishes the outward heat transfer from the pipelines. Concurrently, the outer-wall temperature of the insulation layer demonstrates an ascending trend with increasing ambient temperatures, resulting in gradual decreases in both Q_{FL} and Q_{GB}. These parameters exhibit identical reduction rates under temperature variations, maintaining ε constant at 0.64%. For every 5 K increase in ambient temperature, heat loss decreases by 1.44 W/m^2.

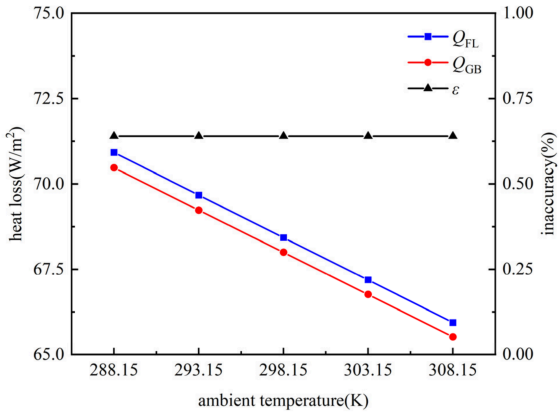


Figure 12. Effect of ambient temperature on heat loss.

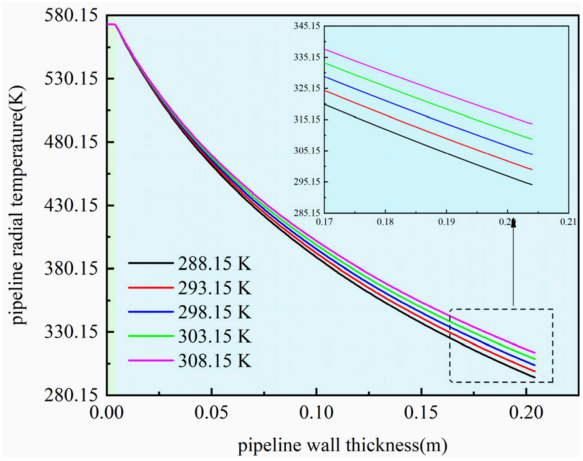


Figure 13. Radial temperature distributions at different ambient temperatures.

3.5. Sunlight Radiation

The influence of sunlight radiation intensity on heat loss is illustrated in Figure 14. Under no-light conditions, the value of Q_{FL} is slightly higher than Q_{GB}. As sunlight intensity increases, Q_{FL} gradually decreases, while Q_{GB} remains constant, causing the ε to progressively rise. Figure 15 demonstrates radial temperature distributions under varying sunlight radiation intensities. Under sunlight radiation, sunlight irradiating the outer surface of the insulation layer introduces an additional heat flux. Concurrently, heat transfers from the inner pipe wall to the insulation outer wall, while sunlight radiation drives heat flux from the outer wall inward. When these dual heat transfer mechanisms reach equilibrium, the steady-state radial temperature distributions shown in Figure 15 are established. As sunlight intensity increases, the outer-wall temperature of the insulation layer rises from 304 K to 344.91 K, while Q_{FL} decreases from 68.43 W/m^2 to 58.03 W/m^2. For every 100 W/m^2 increase in sunlight intensity, heat loss decreases by 1.30 W/m^2. In contrast, the GB method measures heat loss under no-light conditions, yielding a constant Q_{GB} of 68 W/m^2. This discrepancy amplifies the ε from 0.64% to 15.30% as sunlight intensity increases. Consequently, the actual heat loss in steam injection pipelines decreases under sunlight exposure. However, the GB method neglects sunlight radiation effects, rendering it unsuitable for scenarios involving sunlight.

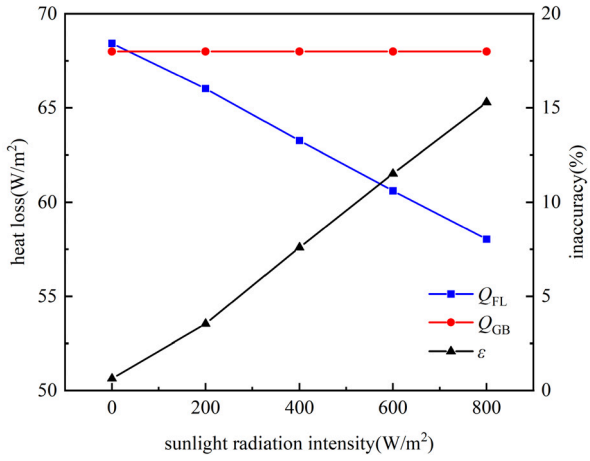


Figure 14. Effect of sunlight radiation intensity on heat loss.

The national standard method for calculating heat loss is not applicable to conditions with sunlight. To facilitate the calculation of heat loss under sunlight conditions, based on

numerical simulation data, a heat loss calculation formula suitable for sunlight conditions is proposed. The form of the formula is shown in Equation (13):

$$Q_{\text{Sunlight}} = h_{\text{Sunlight}}(T_{\text{wall,out}} - T_{\text{Air}}) \tag{13}$$

where Q_{Sunlight} is the heat loss per unit area under light conditions, W/m^2; and h_{Sunlight} is the heat transfer coefficient, W/(m^2·K) and is dependent on T_{Air} (ambient temperature) and E_{Sunlight} (sunlight intensity).

The form of the heat loss calculation formula under sunlight conditions is the same as the national standard method, but the difference lies in the calculation method of the convective heat transfer coefficient h_{Sunlight}. This paper simulates the working conditions of steam injection pipelines under various sunlight intensities at different ambient temperatures, calculates the heat loss, and fits the calculation method of the heat transfer coefficient h_{Sunlight} under sunlight conditions, as shown in Equation (14):

$$h_{\text{Sunlight}} = \frac{0.5071E_{\text{Sunlight}} - 9.5681T_{\text{Air}} - 2285.3457}{-4.4075E_{\text{Sunlight}} - 433.7002} \tag{14}$$

where E_{Sunlight} is sunlight intensity; and W/m^2; T_{Air} is the ambient temperature, K. Equation (14) applies to E_{Sunlight} values ranging from 0 W/m^2 to 800 W/m^2 and T_{Air} values ranging from 273.15 K to 303.15 K.

The coefficient of R^2 for Equation (14) is 0.9951, with an average error of 5.57%, demonstrating the equation's excellent computational accuracy. Figure 16 shows the fitted surface for h_{Sunlight} and the distribution of true value points. The surface closely matches the data points, indicating a high-quality fit.

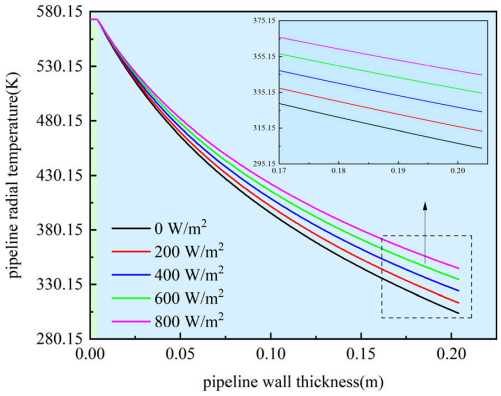


Figure 15. Radial temperature distributions at different sunlight radiation intensities.

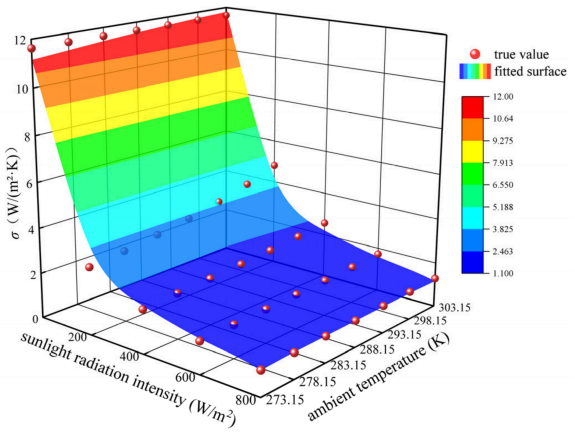


Figure 16. Fitted surface for heat transfer coefficient h_{Sunlight}.

3.6. Comparison of Overhead and Buried Pipelines

A comparison between overhead and buried pipelines is presented in Table 2. Under identical parameters, the outer-wall temperature of the insulation layer in buried pipelines is higher than that of overhead pipelines, and the former exhibits lower heat loss. This is attributed to the surrounding soil acting as an additional insulation layer, which reduces the heat transfer rate and elevates the outer-wall temperature of the insulation layer in buried pipelines. Consequently, buried steam injection pipelines exhibit lower heat loss compared to overhead pipelines. Additionally, under identical operating conditions, variations in relevant parameters (e.g., thermal conductivity, ambient temperature) result in similar trends in heat loss and outer-wall temperature changes for both pipeline types. The heat loss law of buried pipelines aligns with those of overhead pipelines under dynamic parameter adjustments.

Table 2. Comparison of overhead and buried pipelines.

Ambient Temperature (K)	Insulation Conductivity (W/(m·K))	Steam Temperature (K)	Outer-Wall Temperature (K)		Heat Loss (W/m^2)	
			Overhead	Buried	Overhead	Buried
288.15	0.100	573.15	294.21	318.04	70.92	64.86
293.15			299.10	322.51	69.67	63.72
298.15			304.00	326.99	68.43	62.59
303.15			308.89	331.46	67.19	61.45
308.15			313.78	335.94	65.94	60.31
298.15	0.050	573.15	301.10	313.39	34.59	33.02
	0.075		302.55	320.38	51.60	48.20
	0.100		304.00	326.99	68.43	62.59
	0.125		305.42	333.25	85.08	76.24
	0.150		306.84	339.20	101.56	89.22
298.15	0.100	533.15	303.15	322.79	58.48	53.48
		553.15	303.57	324.89	63.45	58.03
		573.15	304.00	326.99	68.43	62.59
		593.15	304.42	329.09	73.41	67.14
		613.15	304.85	331.18	78.38	71.69

3.7. Soil Thermal Conductivity

Heat loss in buried pipelines is not only dependent on the insulation performance of the pipelines but is also intimately linked to the thermal conductivity of the surrounding soil. As depicted in Figure 17, the influence of soil thermal conductivity on the outer-wall temperature of the insulation layer and heat loss in buried pipelines is illustrated. The figure demonstrates that higher soil thermal conductivity results in a lower outer-wall temperature of the insulation layer and, consequently, greater heat loss. This occurs because the soil surrounding the pipelines directly affects heat dissipation. A higher soil thermal conductivity accelerates the heat transfer rate, facilitating faster heat diffusion from the pipelines to the surrounding soil. This process lowers the outer-wall temperature of the insulation layer, leading to increased heat loss. Conversely, lower thermal conductivity reduces the heat transfer rate, enabling the soil to act as an additional insulating layer. This elevates the outer-wall temperature of the insulation and reduces heat loss.

For instance, when the soil thermal conductivity increases from 0.8 W/(m·K) to 1.6 W/(m·K), the outer-wall temperature of the insulation layer decreases from 338.28 K to 320.90 K, while heat loss rises from 59.71 W/m^2 to 64.13 W/m^2. Soil looseness, type, and moisture content are the three primary factors influencing its thermal conductivity. These factors collectively determine thermal performance by altering soil pore structure, heat transfer media, and particle contact mechanisms. In engineering applications, it is advisable

to select soils with low thermal conductivity, regulate looseness and moisture content, and dynamically monitor environmental changes that may perturb thermal conductivity to mitigate heat loss.

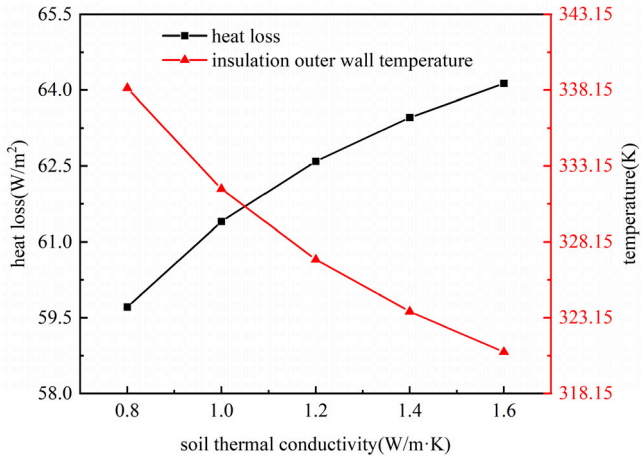


Figure 17. Effect of soil thermal conductivity on buried pipelines.

3.8. Comparison of Buried Pipelines with and Without Insulation

The buried pipeline and soil temperature distribution curves are shown in Figure 18. When the soil burial depth is 1.8 m, the steam temperature is 573.15 K and the ambient temperature is 273.15 K. The surface soil temperature of the buried pipeline with insulation is 274.04 K, while that of the buried pipeline without insulation is 284.43 K, which is significantly higher than that of the pipeline with insulation. The outer surface temperature of the insulation of the buried pipeline with insulation is 292.17 K, while the soil temperature at the same location for the buried pipeline without insulation is 490.60 K. When the surface temperature of the soil is significantly higher than the ambient temperature, it indicates that the insulation layer of the buried pipeline may have been damaged due to corrosion.

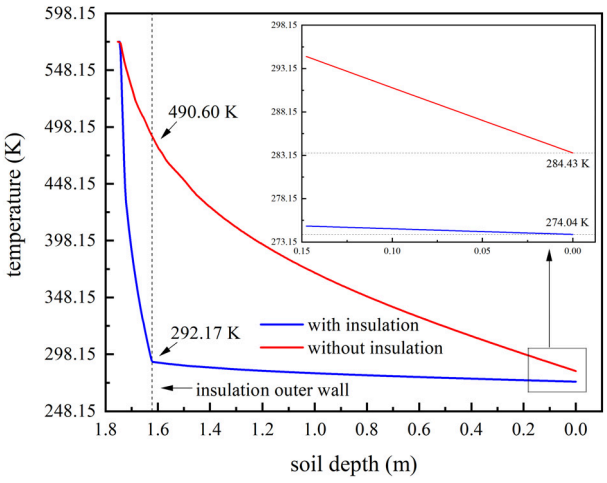


Figure 18. Buried pipeline and soil temperature distribution curves.

4. Conclusions

To investigate the heat transfer characteristics and heat loss influencing factors of steam injection pipelines under various conditions, a three-dimensional numerical model was established. Through parameter comparison and mechanistic analysis, the following conclusions were drawn:

(1) For overhead steam injection pipelines, insulation parameters strongly control radial heat loss. When the insulation thermal conductivity increased from 0.05 to 0.15 W/(m·K), the heat loss increased by approximately 6.7 W/m^2 for every 0.01 W/(m·K) increment. Increasing the insulation thickness from 0.20 to 0.30 m reduced heat loss from 68.43 to 40.79 W/m^2, but the marginal reduction decreased from 3.38 to 2.14 W/m^2 per 0.01 m, indicating a diminishing return. Therefore, low-conductivity insulation and an economically reasonable thickness should be prioritized in steam injection networks;

(2) Sunlight radiation has a measurable positive effect on reducing actual heat loss from overhead pipelines. As sunlight radiation intensity increased from 0 to 800 W/m^2, the insulation outer-wall temperature increased from 304.00 to 344.91 K, while the actual heat loss decreased from 68.43 to 58.03 W/m^2, corresponding to a reduction of about 15.2%. The fitted sunlight-dependent coefficient h_{Sunligh} (E, T) achieved R^2 = 0.9951 and an average error of 5.57%, providing a practical correction for sunlight heat loss evaluation;

(3) Installation configuration and soil properties also significantly influence heat loss. Under the same operating conditions, buried pipelines exhibited a heat loss of 62.59 W/m^2, which was 8.5% lower than that of overhead pipelines. When soil thermal conductivity increased from 0.8 to 1.6 W/(m·K), buried pipeline heat loss increased from 59.71 to 64.13 W/m^2. For buried pipelines without insulation, the calculated soil temperature at the location corresponding to the insulation outer surface reached 490.60 K, much higher than the 292.17 K for insulated pipelines, indicating that abnormal ground surface temperature can be used as a warning signal for insulation damage.

Author Contributions: Conceptualization, P.A. and G.G.; Data curation, Y.Q. and J.Z.; Formal analysis, P.A. and J.L.; Funding acquisition, X.W.; Investigation, Z.M.; Methodology, Y.Q. and Z.M.; Project administration, J.Z.; Resources, X.W.; Software, P.A. and Y.Q.; Supervision, G.G.; Validation, J.L. and J.Z.; Visualization, J.L.; Writing—original draft, P.A. and J.L.; Writing—review and editing, Y.Q. and X.W. All authors have read and agreed to the published version of the manuscript.

Funding: This work is supported by the National Natural Science Foundation of China (52476143).

Institutional Review Board Statement: Not applicable.

Informed Consent Statement: Not applicable.

Data Availability Statement: The data that support the findings of this study are available from the corresponding author upon reasonable request.

Conflicts of Interest: Authors Paerhati Abudukelimu, Genying Gao, Jianping Zhou, and Zhongshan Ma were employed by the Research Institute of Oil Production Technology, Petro China Xinjiang Oilfield Company, and Junde Liu was employed by the Infrastructure Engineering Department, Petro China Xinjiang Oilfield Company. The remaining authors declare that the research was conducted in the absence of any commercial or financial relationships that could be construed as a potential conflict of interest.

Nomenclature

Symbols:

A	area (m^2)
d_1	pipeline inner diameter (m)
d_2	pipeline outer diameter(m)
d_3	insulation outer diameter (m)
l	pipeline length (m)
Q	heat loss (W/m^2)
T	temperature (K)

Greek symbols:

ε	deviation (%)
λ_1	pipeline thermal conductivity (W/(m·K))
λ_2	insulation thermal conductivity (W/(m·K))
ω	wind speed (m/s)
φ	heat flux (W)
h	heat transfer coefficient (W/(m^2·K))

Subscripts:

FL	Fourier's law
GB	GB/T 17357-2008
Sunlight	sunlight conditions
wall,in	pipeline inner wall temperature
wall,out	insulation outer-wall temperature
Air	ambient temperature

References

1. Jadidi, S.A.; Moolya, S.; Satheesh, A. Analysis of Core Annular Flow Behavior of Water-Lubricated Heavy Crude Oil Transport. *Fluids* **2023**, *8*, 267. [CrossRef]
2. Dengaev, A.V.; Khelkhal, M.A.; Getalov, A.A.; Baimukhametov, G.F.; Kayumov, A.A.; Vakhin, A.V.; Gafurov, M.R. Innovations in Oil Processing: Chemical Transformation of Oil Components through Ultrasound Assistance. *Fluids* **2023**, *8*, 108. [CrossRef]
3. Fan, Y.; Li, H.; Duan, S.; Gu, P.; Ren, N. Concentrated solar steam generation technology enables low carbon shallow super-heavy oil production. *Xinjiang Oil Gas* **2023**, *19*, 82–87. [CrossRef]
4. Wang, P.; Liu, Y.; Liang, X.; Zheng, A.; Qin, N. Numerical simulation of nitrogen-assisted vhsd development in old super-heavy oil reservoirs. *Xinjiang Oil Gas* **2024**, *20*, 38–43. [CrossRef]
5. Miao, Y.; Zhao, Q.; Huang, Z.; Zhao, K.; Zhao, H.; Guo, L.; Wang, Y. Core flooding experimental study on enhanced oil recovery of heavy oil reservoirs with high water cut by sub- and supercritical water. *Geoenergy Sci. Eng.* **2024**, *242*, 213208. [CrossRef]
6. Zhang, L.; You, H.; Su, R.; Guo, W. Experimental research and application of VHSD dilatation stimulation in shallow heavy oil reservoirs. *Xinjiang Oil Gas* **2023**, *19*, 69–74. [CrossRef]
7. Satar, V.; Ozturk, H. Economic analysis of steam assisted underground mining of Bati Raman heavy oil field. *Geoenergy Sci. Eng.* **2024**, *235*, 212714. [CrossRef]
8. Pirouti, M.; Bagdanavicius, A.; Ekanayake, J.; Wu, J.; Jenkins, N. Energy consumption and economic analyses of a district heating network. *Energy* **2013**, *57*, 149–159. [CrossRef]
9. Başoğul, Y.; Keçebaş, A. Economic and environmental impacts of insulation in district heating pipelines. *Energy* **2011**, *36*, 6156–6164. [CrossRef]
10. Werner, S. Network configurations for implemented low-temperature district heating. *Energy* **2022**, *254*, 124091. [CrossRef]
11. Başoğul, Y.; Demircan, C.; Keçebaş, A. Determination of optimum insulation thickness for environmental impact reduction of pipe insulation. *Appl. Therm. Eng.* **2016**, *101*, 121–130. [CrossRef]
12. Keçebas, A. Determination of insulation thickness by means of exergy analysis in pipe insulation. *Energy Convers. Manag.* **2012**, *58*, 76–83. [CrossRef]
13. Lahmer, E.; Moussaoui, M.A.; Bode, F.; Mezrhab, A. Quality of heat transfer assessment of two microprocessors by double-layered mini channel heat sink cooling system for moderate Reynolds number. *Therm. Sci. Eng. Prog.* **2023**, *41*, 101804. [CrossRef]
14. Lahmer, E.; Benhamou, J.; Elouazzani, M.A.; Moussaoui, M.A.; Ahmed Mezrhab, A. Heat transfer enhancement of a microchannel cooler with V-shaped partitions. *Int. J. Thermofluids* **2023**, *20*, 100450. [CrossRef]
15. Lahmer, E.; Benhamou, J.; Admi, Y.; Moussaoui, M.A.; Mezrhab, A.; Phanden, R.K. Evaluation of heat transfer rate of double-layered heat sink cooling system with high energy dissipation. *J. Enhanc. Heat Transf.* **2024**, *31*, 19–37. [CrossRef]
16. Anand, S.; Bansal, N.K.; Park, S.R.; Tyagi, S.K. Comparative study of different insulating materials for reducing the heat losses in steam pipes: A technical study. *Int. J. Sustain. Energy* **2012**, *31*, 133–141. [CrossRef]
17. Lin, J.; Zhao, J.; Wang, X.; Chen, K.; Zhang, L. Field experimental investigation of the insulation deterioration characteristics of overhead pipeline for steam heating network. *J. Enhanc. Heat Transf.* **2024**, *31*, 17–31. [CrossRef]
18. Wang, D. Heat loss along the pipeline and its control measures. *SN Appl. Sci.* **2022**, *5*, 2. [CrossRef]
19. Příhoda, M.; Čarnogurská, M.; Pyszko, R.; Hlisnikowski, E.; Burda, J. Heat Loss Analysis of Outdoor Piping. *MATEC Web Conf.* **2020**, *328*, 03006. [CrossRef]
20. Alrasheed, M.R.A. Optimizing the Thickness of Multilayer Thermal Insulation on Different Pipelines for Minimizing Overall Cost-Associated Heat Loss. *Processes* **2024**, *12*, 318. [CrossRef]

21. Kruczek, T. Determination of annual heat losses from heat and steam pipeline networks and economic analysis of their thermo-modernisation. *Energy* **2013**, *62*, 120–131. [CrossRef]
22. Danielewicz, J.; Sniechowska, B.; Sayegh, M.-A.; Fidorow, N.; Jouhara, H. Three-dimensional numerical model of heat losses from district heating network pre-insulated pipes buried in the ground. *Energy* **2016**, *108*, 172–184. [CrossRef]
23. Bøhm, B. On transient heat losses from buried district heating pipes. *Int. J. Energy Res.* **2000**, *24*, 1311–1334. [CrossRef]
24. Schörghofer, N.; Khatiwala, S. Semi-implicit Solver for the Heat Equation with Stefan–Boltzmann Law Boundary Condition. *Planet. Sci. J.* **2024**, *5*, 120. [CrossRef]
25. *GB/T 17357*; In-situ Measurements of Heat Loss Through Thermal Insulation of Equipments and Pipes-heat Flow Meter Apparatus and Surface Temperature Method. China Standards Press: Beijing, China, 2008.
26. Wang, Y.; Wang, P. Application of Fourier's Law in One-Dimensional Steady Heat Conduction Calculation of Cylinder Wall. *J. Phys. Conf. Ser.* **2022**, *2381*, 012002. [CrossRef]

Disclaimer/Publisher's Note: The statements, opinions and data contained in all publications are solely those of the individual author(s) and contributor(s) and not of MDPI and/or the editor(s). MDPI and/or the editor(s) disclaim responsibility for any injury to people or property resulting from any ideas, methods, instructions or products referred to in the content.